

## Electronic Supplementary Information

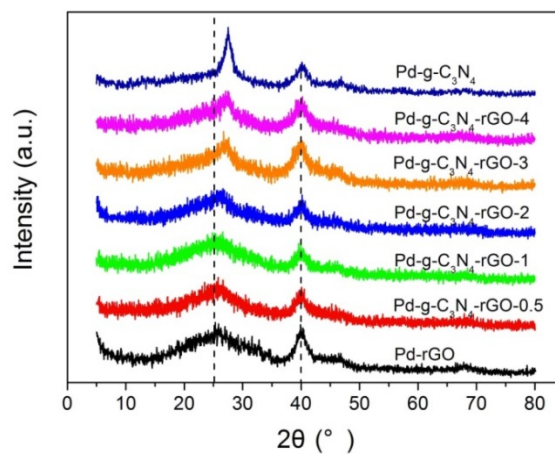


Fig.S1 XRD patterns of Pd-g-C<sub>3</sub>N<sub>4</sub>, Pd-rGO and Pd-g-C<sub>3</sub>N<sub>4</sub>-rGO-n (n=0.5, 1, 2, 3, 4).

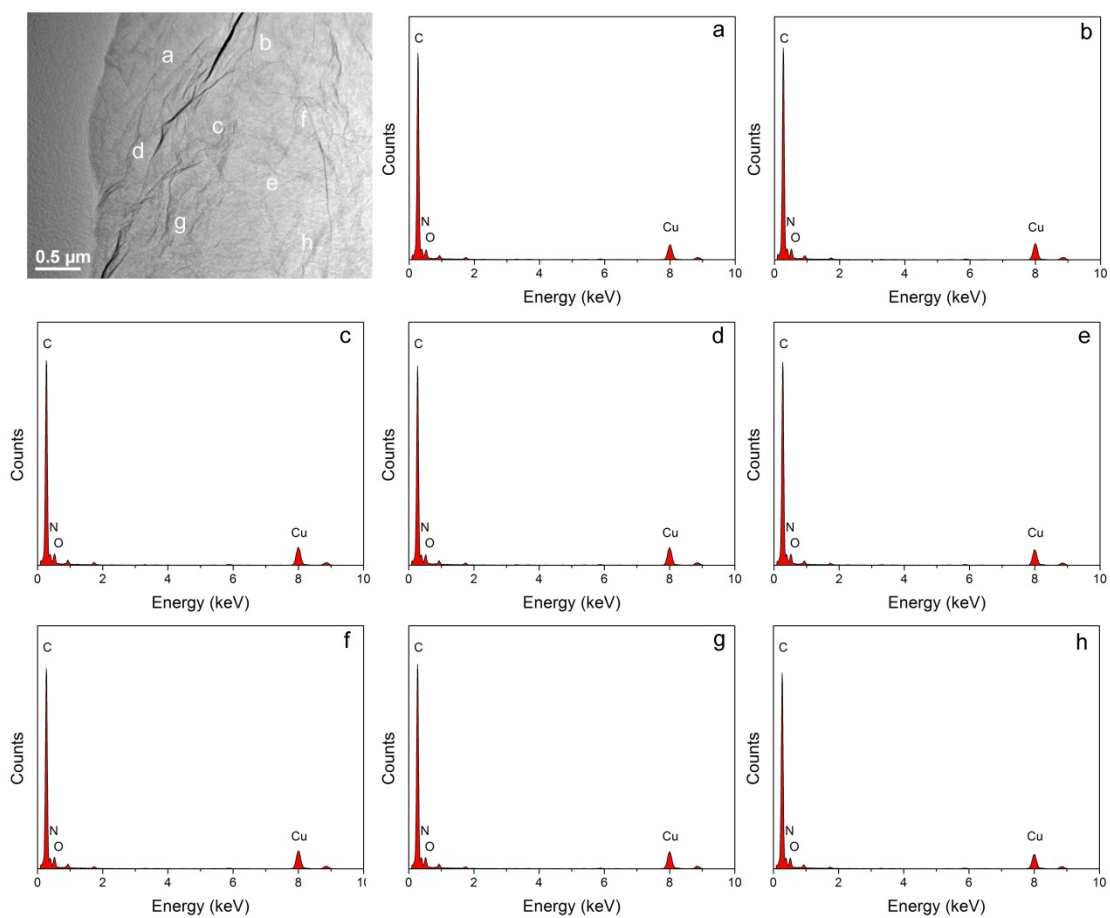


Fig. S2 Typical TEM image of g-C<sub>3</sub>N<sub>4</sub>-rGO-2 and the energy dispersive X-ray spectrum corresponding to the random areas in the TEM image.

Table S1. C, O and N content (at%) of the g-C<sub>3</sub>N<sub>4</sub>-rGO-2 at different areas according to EDX analysis. Focusing on random areas of the sample, a signal of N element is clearly observable and the corresponding N contents of different areas are almost the same, further proving the uniform distribution of g-C<sub>3</sub>N<sub>4</sub> on the surface of rGO.

	Element content (at%)		
	C	N	O
a	93.50	4.30	2.20
b	93.40	4.30	2.30
c	93.10	4.40	2.50
d	93.30	4.30	2.40
e	93.40	4.30	2.30
f	92.90	4.50	2.50
g	93.20	4.40	2.40
h	93.30	4.30	2.40

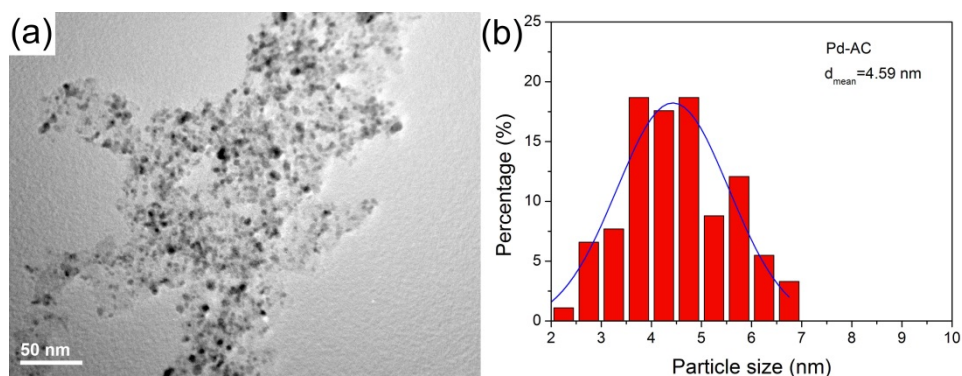


Fig. S3 (a) TEM images of Pd-AC, (b) Histograms of Pd particle size distribution of Pd-AC.

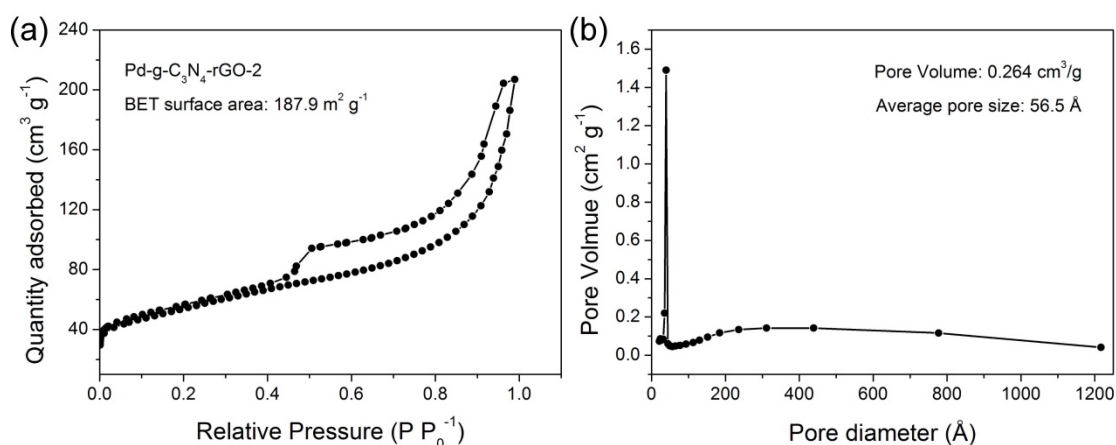


Fig. S4 (a) Nitrogen adsorption-desorption isotherms and (b) the corresponding pore-size distribution of Pd-g-C<sub>3</sub>N<sub>4</sub>-rGO-2, respectively, confirm the mesoporous features with high surface area.

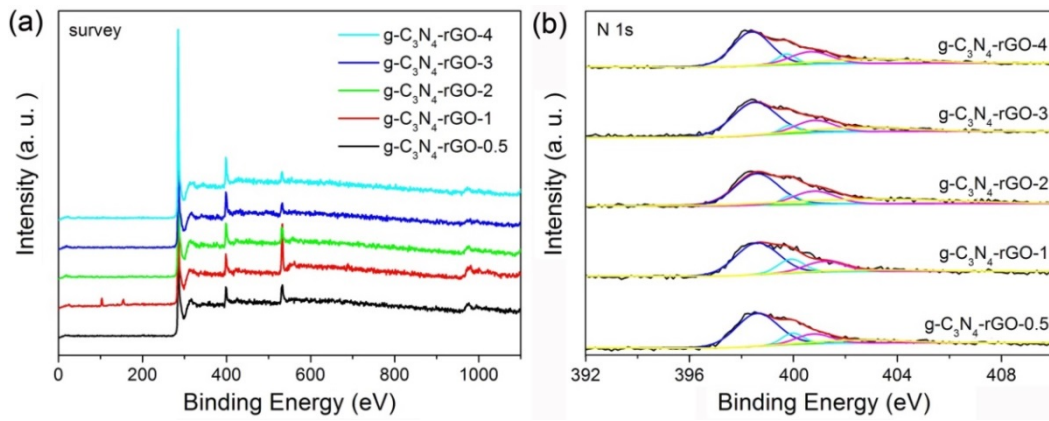


Fig. S5 (a) XPS survey spectra, (b) N 1s core-level XPS spectra of g-C<sub>3</sub>N<sub>4</sub>-rGO-n prepared by annealing GO and melamine under different mass ratio. With the atomic percentage of nitrogen increasing, the four components of nitrogen increases at the same time.

Table S2. Elemental Composition of g-C<sub>3</sub>N<sub>4</sub>-rGO Prepared by Annealing GO and Melamine under Different Mass Ratio.

Samples	C at%	N at%	O at%	N/C
g-C <sub>3</sub> N <sub>4</sub> -rGO-0.5	87.9	6.5	5.6	0.074
g-C <sub>3</sub> N <sub>4</sub> -rGO-1	83.1	8.1	10.5	0.097
g-C <sub>3</sub> N <sub>4</sub> -rGO-2	86.5	9.5	4.9	0.110
g-C <sub>3</sub> N <sub>4</sub> -rGO-3	86.2	10.3	3.5	0.119
g-C <sub>3</sub> N <sub>4</sub> -rGO-4	85.7	11	3.3	0.128

As listed in Table S1, with the amount of melamine increasing, the calculated N/C atomic ratio ranges from 0.074 to 0.128, owing to more formation of g-C<sub>3</sub>N<sub>4</sub> layers on the surface of graphene.

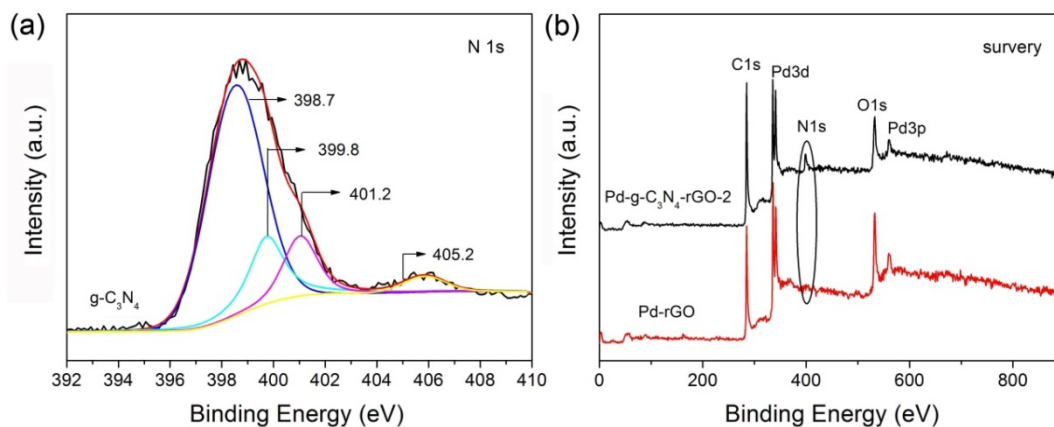


Fig. S6 (a) N 1s core-level XPS spectra of g-C<sub>3</sub>N<sub>4</sub>, (b) XPS survey spectra of the Pd-g-C<sub>3</sub>N<sub>4</sub>-rGO-2 and Pd-rGO samples. The survey spectra (Fig. S6b) distinctly confirms the incorporation of nitrogen atoms within the final Pd-g-C<sub>3</sub>N<sub>4</sub>-rGO-2 composite. Conversely, the XPS spectrum of Pd-rGO presents only the existence of Pd, C and O elements.

Table S3. The percent of different Pd valence states from the fitting curves of Pd 3d XPS spectra.

Samples	Pd species	
	Pd <sup>0</sup> (at %)	Pd <sup>2+</sup> (at %)
Pd-g-C <sub>3</sub> N <sub>4</sub> -rGO-2	80.1	19.9
Pd-rGO	73.6	26.4

Table S4. The g-C<sub>3</sub>N<sub>4</sub> content in different ternary catalysts, based on the XPS analysis.

Samples	g-C <sub>3</sub> N <sub>4</sub> wt%
Pd-g-C <sub>3</sub> N <sub>4</sub> -rGO-0.5	6.5
Pd-g-C <sub>3</sub> N <sub>4</sub> -rGO-1	7.5
Pd-g-C <sub>3</sub> N <sub>4</sub> -rGO-2	9.2
Pd-g-C <sub>3</sub> N <sub>4</sub> -rGO-3	12.1
Pd-g-C <sub>3</sub> N <sub>4</sub> -rGO-4	13.6

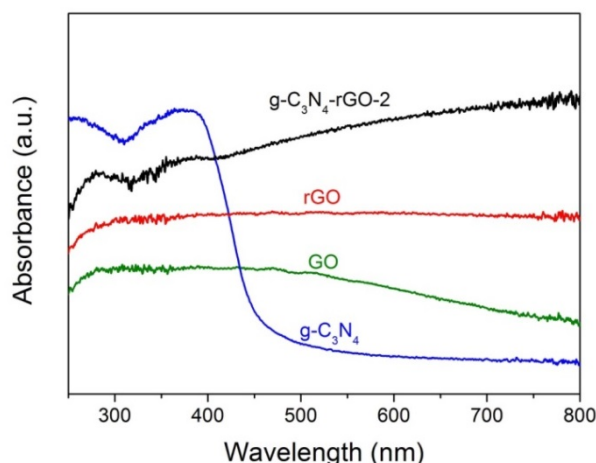


Fig. S7 UV-vis spectra of  $g\text{-C}_3\text{N}_4\text{-rGO-2}$ , rGO, GO and  $g\text{-C}_3\text{N}_4$ .

Fig. S7 shows the UV-vis spectra of  $g\text{-C}_3\text{N}_4$ , GO, rGO and  $g\text{-C}_3\text{N}_4\text{-rGO-2}$ . Generally, the bare  $g\text{-C}_3\text{N}_4$  could exhibit distinct adsorption only in the UV region but limited in the VL region, and rGO could exhibit strong adsorption both in the UV and VL region. However, the  $g\text{-C}_3\text{N}_4\text{-rGO-2}$  not only has a strong adsorption in the entire region, but also has a significant enhancement in UV region, which provides another evidence for the combination of  $g\text{-C}_3\text{N}_4$  layers and graphene sheets.

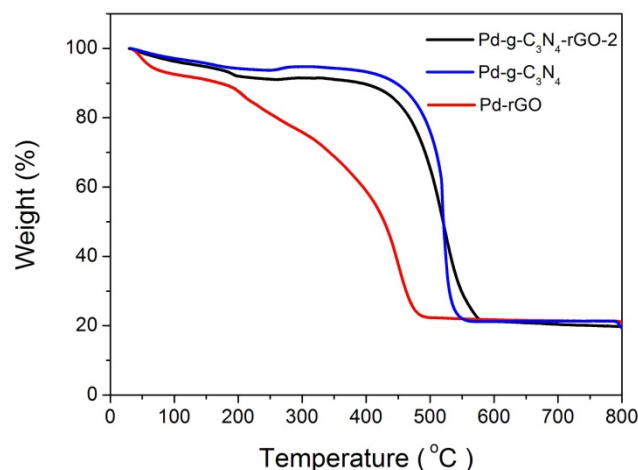


Fig. S8 TG analysis of  $\text{Pd-g-C}_3\text{N}_4\text{-rGO-2}$ ,  $\text{Pd-g-C}_3\text{N}_4$  and  $\text{Pd-rGO}$ .

The TG analyses of the  $\text{Pd-g-C}_3\text{N}_4\text{-rGO-2}$ ,  $\text{Pd-g-C}_3\text{N}_4$  and  $\text{Pd-rGO}$  samples were carried out under an air atmosphere from 30 to 800 °C at a heating rate of  $5\text{ °C}\cdot\text{min}^{-1}$ , as shown in Fig. S8. For all the samples, two major weight losses can be observed in their TG curves. The first weight losses below 200 °C are due to the physically

adsorbed water of the composite, while the second weight losses in the range of 200-600 °C correspond to the degradation of the supporting materials. For all the samples, the residue weight was about 20 % which can be ascribed to the remaining Pd and the mass percentage of Pd is in agree with the ICP results.

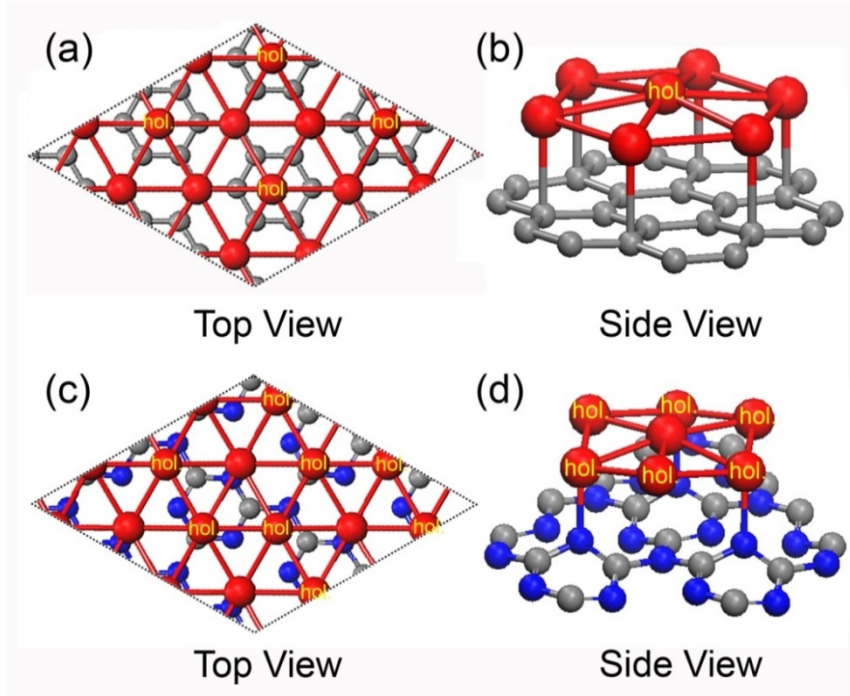


Fig. S9 Geometric structures of (a, b) graphene and (c, d) g-C<sub>3</sub>N<sub>4</sub>. The big red, small grey and blue balls represent Pd, C and N atoms, respectively.

$2\sqrt{3} \times 2\sqrt{3}$  unit cell of Pd within a fcc structure in the (111) orientation is used to accommodate a  $4 \times 4$  unit cell of the graphene and g-C<sub>3</sub>N<sub>4</sub> (C<sub>32</sub>Pd<sub>12</sub> and C<sub>12</sub>N<sub>16</sub>Pd<sub>12</sub>). This leads to 3.3 % tensile strain and 1.2 % compressive strain, respectively. For graphene, the optimized average distance of the Pd to the graphene is 2.48 Å, agrees well with the reported 2.49 Å<sup>[1]</sup>. While for g-C<sub>3</sub>N<sub>4</sub>, the missing C atoms in g-C<sub>3</sub>N<sub>4</sub> structure would weaken the layers contact between Pd and C atoms, which is compensated by the strong Pd-N bonding of only 2.08 Å. As a result, the average distance between g-C<sub>3</sub>N<sub>4</sub> and Pd<sub>top</sub> increases a little larger to 2.52 Å, and the distance between g-C<sub>3</sub>N<sub>4</sub> and Pd<sub>hollow</sub> is significantly increased to 2.96 Å.

The charge density difference is defined as  $\Delta\rho = \rho_{\text{Pd/substrate}} - \rho_{\text{substrate}} - \rho_{\text{Pd}}$  (substrate = graphene, g-C<sub>3</sub>N<sub>4</sub>). Here,  $\rho_{\text{Pd/substrate}}$ ,  $\rho_{\text{substrate}}$ ,  $\rho_{\text{Pd}}$  represent the charge

density of the Pd covering on the substrate, the substrate layer and the Pd freestanding layer, respectively. Moreover, the absorptive energy is defined as  $E_{\text{abs}} = E_{\text{Pd/substrate}} - E_{\text{substrate}} - E_{\text{Pd}}$  (substrate = graphene, g-C<sub>3</sub>N<sub>4</sub>). Here,  $E_{\text{Pd/substrate}}$ ,  $E_{\text{substrate}}$ ,  $E_{\text{Pd}}$  represent the structure energy of the Pd covering on the substrate, the substrate layer and the Pd freestanding layer, respectively.

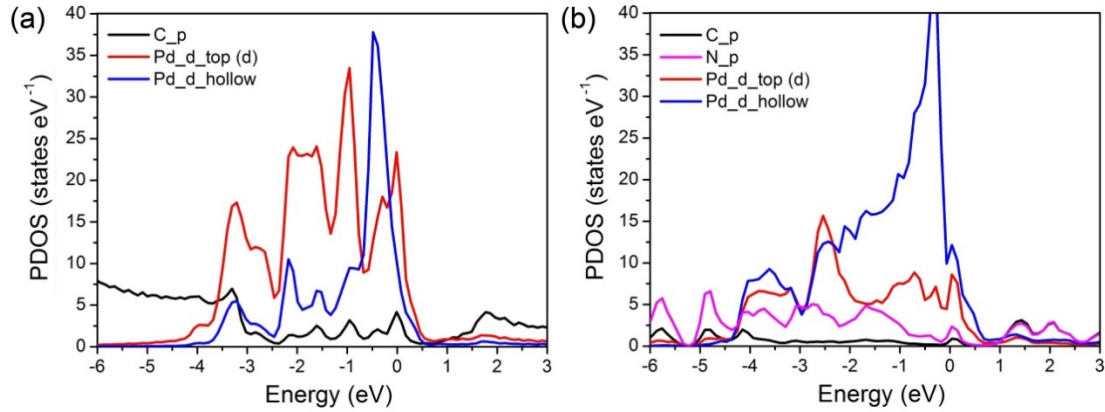


Fig. S10 Partial density of states (PDOS) plots of Pd layer on (a) graphene and (b) g-C<sub>3</sub>N<sub>4</sub>. The red curves and the blue curves are the d orbital of the Pd atoms located at top and hollow site, respectively. Black and pink curves are the p orbital of C and N atoms. The Fermi energy is set at zero.

In order to explore more details of the electronic structures, the PDOSs are displayed in Fig. S10. For graphene, the overlaps between C<sub>p</sub> and Pd<sub>d\_top</sub> at around -0.1 eV, -1.0 eV, -2.2 eV and -3.2 eV indicate the strong valence bonds between the C atoms and Pd<sub>top</sub> atoms, while the bonding is relatively weaker between the Pd<sub>hollow</sub> and C atoms, due to the longer distance from 2.52 Å to 2.96 Å. For g-C<sub>3</sub>N<sub>4</sub>, the N doping and the missing C atoms have significantly reduced the C-Pd<sub>top</sub> bonding, which is compensated by the strong N-Pd<sub>top</sub> valence bonding. Typically, the peak of the p orbital of N atoms located at about -1.4 eV and the wide overlaps between N<sub>p</sub> and Pd<sub>d\_top</sub>. Therefore, the hybridizations among Pd, C and N atoms significantly affect the electronic structures, driving the Pd atoms anchor onto the g-C<sub>3</sub>N<sub>4</sub> substrate.

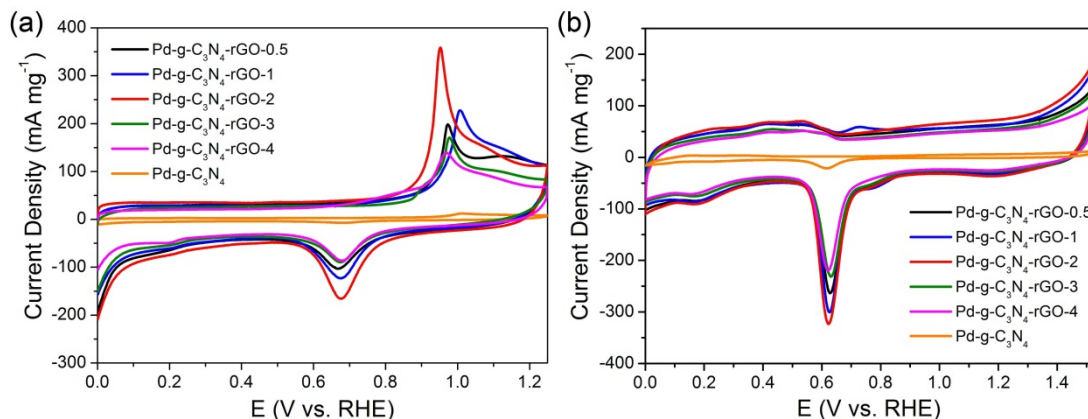


Fig. S11 (a) CO<sub>ad</sub> stripping voltammograms for different catalysts in 0.5 M H<sub>2</sub>SO<sub>4</sub> solution with a scan rate of 50 mV·s<sup>-1</sup>, (b) CVs of different catalysts in 1 M NaOH solutions with a scan rate of 50 mV·s<sup>-1</sup>.

Either in alkaline medium or acid medium, Pd-g-C<sub>3</sub>N<sub>4</sub> shows a low ECSA values. This may due to the poor electrical conductivity of g-C<sub>3</sub>N<sub>4</sub> support material, which makes it difficult for electronic transmission, consequently results in low catalytic sites and in turn, electrooxidative activity for methanol and formic acid Fig. S11).

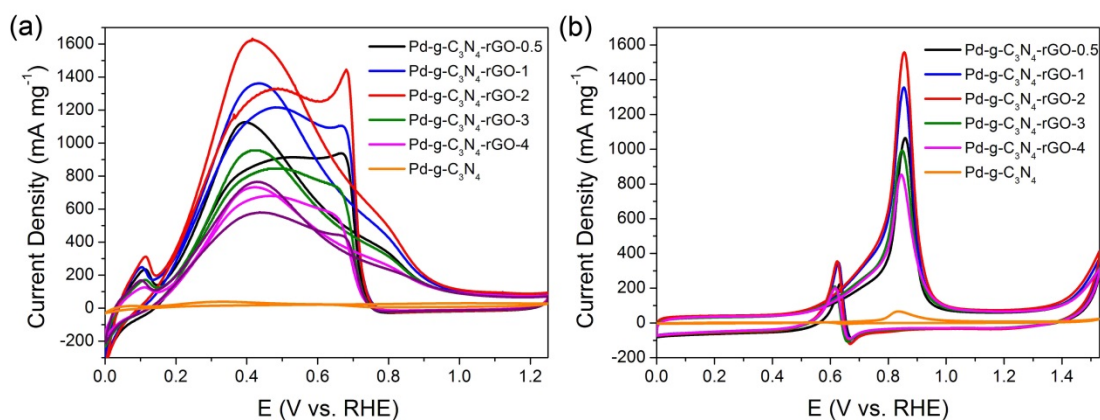


Fig. S12 CVs of different catalysts in (a) 0.5 M H<sub>2</sub>SO<sub>4</sub> with 0.5 M HCOOH solution, (b) 1 M NaOH with 1 M CH<sub>3</sub>OH with a scan rate of 50 mV·s<sup>-1</sup> at 25 °C.

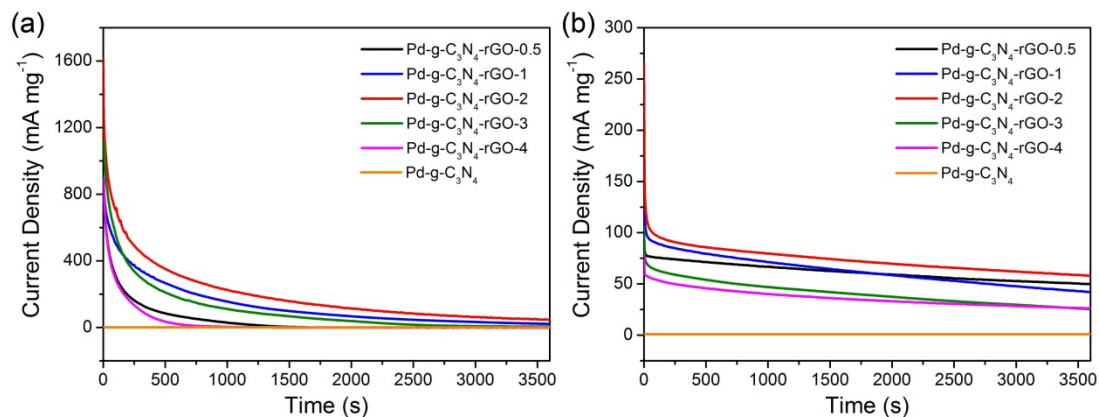


Fig. S13 Chronoamperometric curves of different catalysts in (a) 0.5 M  $\text{H}_2\text{SO}_4$  with 0.5 M  $\text{HCOOH}$  solution at 0.4 V, (b) 1 M  $\text{NaOH}$  with 1 M  $\text{CH}_3\text{OH}$  with a scan rate of  $50 \text{ mV} \cdot \text{s}^{-1}$  at 0.7 V at  $25^\circ \text{C}$ .

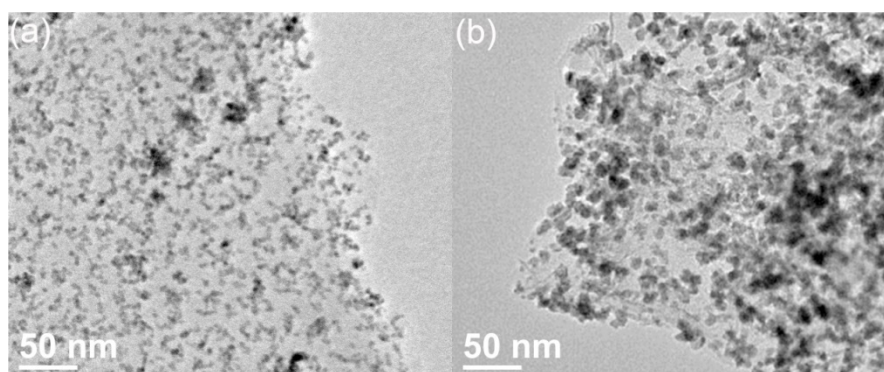


Fig. S14 TEM images of (a)  $\text{Pd-g-C}_3\text{N}_4\text{-rGO-2}$  (b)  $\text{Pd-rGO}$  after immersing in 0.5 M  $\text{H}_2\text{SO}_4$  + 0.5 M  $\text{HCOOH}$  solution for two weeks at  $25^\circ \text{C}$ .

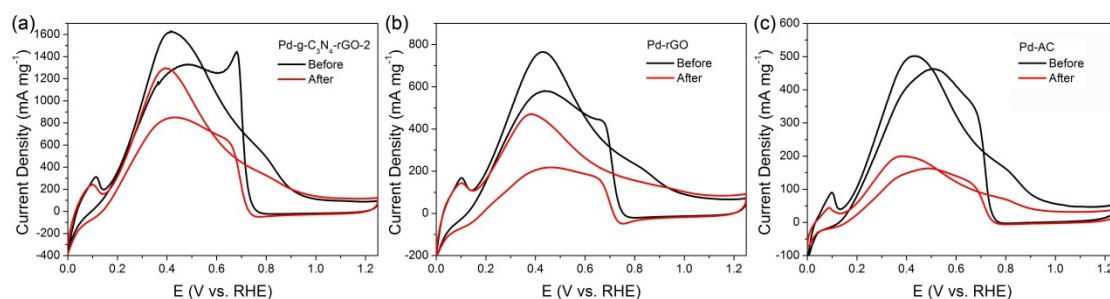


Fig. S15 CV curves on (a)  $\text{Pd-g-C}_3\text{N}_4\text{-rGO-2}$ , (b)  $\text{Pd-rGO}$ , (c)  $\text{Pd-AC}$  catalysts in 0.5 M  $\text{H}_2\text{SO}_4$  with 0.5 M  $\text{HCOOH}$  before and after immersing durability testing at a scan rate of  $50 \text{ mV s}^{-1}$ .

To be more convincing, the  $\text{Pd-g-C}_3\text{N}_4\text{-rGO-2}$ ,  $\text{Pd-rGO}$  and  $\text{Pd-AC}$  catalyst were allowed to immerse in 0.5 M  $\text{H}_2\text{SO}_4$  + 0.5 M  $\text{HCOOH}$  solution for two weeks at  $25^\circ \text{C}$ . After immersing, the size and the dispersion of the Pd nanoparticles in  $\text{Pd-g-C}_3\text{N}_4\text{-rGO-2}$  sample was no significant change except for some slight degree of aggregation

(Fig.S14a). However, in the case of Pd-rGO sample (Fig. S14b), the Pd nanoparticles grew increasingly larger and formed serious aggregates. Additionally, the electrochemically performances were also carried out to investigating the property changes of the electrocatalysts. As seen in Fig. S15, the peak current density on the Pd-g-C<sub>3</sub>N<sub>4</sub>-rGO-2 is 1302 mA mg<sup>-1</sup>, which maintains 80.9 % of the initial current density. In contrast, the Pd-rGO and Pd-AC shows poor catalyze activity maintaining only 61.8 % and 39.8 % of the initial current density. In this regard, we speculate that the g-C<sub>3</sub>N<sub>4</sub> layers on the surface of graphene could strongly anchor Pd nanoparticles and prevent them from conglomerating or dissolving under acid medium.

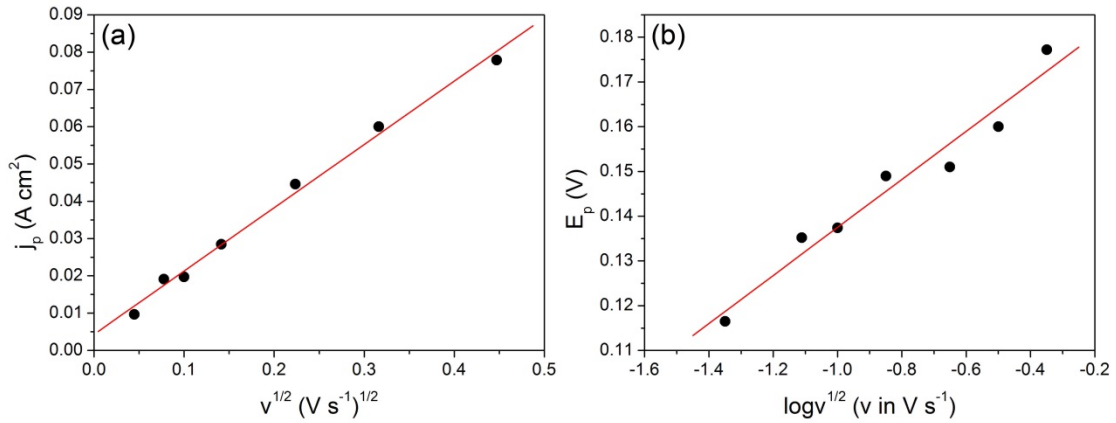


Fig. S16 (a) The plot of the peak current density with square root of scan rate. (b) The plot of the variation of peak potential with logarithm of the square root of scan rate.

In the case of an irreversible reaction, the peak current in amperes is<sup>[2, 3]</sup>:

$$j_p = 2.99 \times 10^5 n(\alpha n')^{1/2} C_0 D_0^{1/2} v^{1/2} \quad (1)$$

where  $n$  is the electron number for the total reaction,  $n'$  is the electron number transferred in the rate-determining step and  $\alpha$  is the charge transfer coefficient. The peak current density  $j_p$  measured in A·cm<sup>-2</sup> and the diffusion coefficient  $D_0$  is in cm<sup>2</sup>·s<sup>-1</sup>. The formic acid concentration is in the solution,  $C_0$ , is in mol·cm<sup>-3</sup> and the sweep rate,  $v$ , is in V·s<sup>-1</sup>.

According to Brett and Brett<sup>[4]</sup>, the relationship between the peak potential ( $E_p$ ) and scan rate ( $v$ ) is defined by the following:

$$\left| \frac{dE_p}{d \log v} \right| = 0.0592 / \alpha n, \quad (2)$$

where  $E_p$  is the peak potential and  $v$  is the scan rate. The value of  $\alpha n'$  can be easily

estimated from the slope of  $E_p$  vs.  $\log v^{1/2}$ .

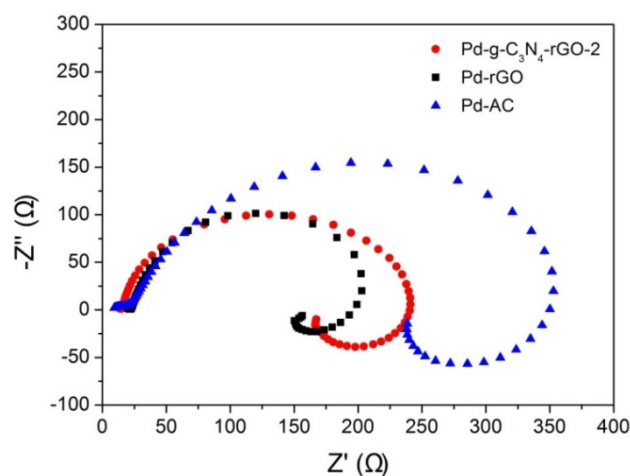


Fig. S17 presents the Nyquist plots of EIS for Pd-g-C<sub>3</sub>N<sub>4</sub>-rGO-2, Pd-rGO and Pd-AC obtained in 1 M NaOH and 1 M CH<sub>3</sub>OH solution at 0.73 V.

Electrochemical impedance spectra (EIS) were performed with amplitude of 5 mV in the frequency range from 10 kHz to 0.01 Hz at a potential of 0.73 V. As seen in Fig. S 17, the EIS plots of all catalysts have the similar semi-cycles, indicating that the mechanism of electrooxidation of methanol on the three catalysts is similar. The diameter of the semicycle can be used to estimate the charge transfer resistance ( $R_{ct}$ ) of the catalyst<sup>[5]</sup>. Typically, the  $R_{ct}$  values in rGO based composites are lower than that in Pd-AC, implying rGO is a more appropriate electrocatalyst support for direct liquid fuel cells. In addition, the appropriate amount of g-C<sub>3</sub>N<sub>4</sub> on the surface of graphene significantly maintains the conductivity of overall electrodes, which is consistent well with the above analyses.

## References

1. Q. J. Wang and J. G. Che, *Phys. Rev. Lett.*, 2009, **103**, 066802.
2. H. Hosseini, M. Mahyari, A. Bagheri and A. Shaabani, *J. Power Sources*, 2014, **247**, 70-77.
3. Y. Wang, B. Wu, Y. Gao, Y. Tang, T. Lu, W. Xing and C. Liu, *J. Power Sources*, 2009, **192**, 372-375.
4. C. M. Brett and A. M. O. Brett, *Electrochemistry: principles, methods, and applications*, Oxford university press Oxford, 1993.
5. H. Huang and X. Wang, *J. Mater. Chem.*, 2012, **22**, 22533-22541.